


Article

Generation of Terahertz OAM Waves with Six Modes Based on Three-Layer Z-Shaped Reflective Metasurface

Qibiao Zhu ^{*}, Xiangzhong Xiao, Lisu Yu  and Nanrun Zhou

Department of Electronic Information Engineering, Nanchang University, Nanchang 330031, China

^{*} Correspondence: zhuqibiao@ncu.edu.cn

Abstract: In this paper, a broadband and efficient three-layer Z-shaped reflective metasurface for linear polarization conversion is designed and six different modes of orbital angular momentum (OAM) waves are generated in the terahertz band. The designed metasurface consisted of several units, and it is divided into twelve regions. The phase difference is achieved by changing the structural parameters of the units, and then different modes of OAM waves are generated. The terahertz OAM waves with the modes of ± 1 , ± 2 , and ± 3 are generated by metasurface with high efficiency and wide bandwidth. The results show that the designed metasurface could produce high purity terahertz OAM waves with six different modes, and the reflection amplitude of the metasurface unit is more than 0.9 in the frequency range of 1.0 THz to 1.8 THz. The generated OAM waves with the modes of ± 1 and ± 2 have a mode purity more than 90%. The designed metasurface has good wavefront control ability, which provides an effective method to generate multimode OAM waves.

Keywords: orbital angular momentum; circular polarization; terahertz; mode purity; reflective metasurface

1. Introduction

With the rapid development of wireless communications, spectrum resources are becoming increasingly absent. Effectively utilizing spectrum resources to meet the rapidly growing demand for spectrums has become a challenge for future communications [1,2]. As a novel spatial multiplexing technique, orbital angular momentum (OAM) is considered to have potential advantages compared to frequency multiplexing such as orthogonal frequency division multiplexing (OFDM) [3]. In 1992, Allen et al. demonstrated that waves can carry orbital angular momentum [4]. OAM macroscopically behaves as a vortex phenomenon of electromagnetic waves [5]. OAM communications have attracted much attention due to their potential to provide additional degrees of freedom for channel capacity [6]. Due to the combination of infinite orthogonal modes and a wide bandwidth, terahertz OAM waves will play an important role in next-generation wireless communications [7].

In 2011, the first experimental test of an OAM technique was successfully carried out, which opened the applications of OAM in the radio field [8]. To realize the practical application of OAM in wireless communications, a high-performance OAM waves generator must be provided. The traditional methods for generating OAM waves mainly include the following: spiral phase plate [9], circular array antenna [10], ring resonator antenna [11]. To obtain the phase conditions required for generating OAM waves, traditional OAM beam-forming methods need complex feeding networks, which make the entire OAM waves generator bulky, and the purity of the OAM waves generated by these traditional methods is too low.

Among the traditional methods for generating OAM waves, the spiral phase plate is a representative method that has been widely used; however, the fabrication of the spiral phase plate is complicated and expensive [12]. To overcome these limitations, researchers



Citation: Zhu, Q.; Xiao, X.; Yu, L.; Zhou, N. Generation of Terahertz OAM Waves with Six Modes Based on Three-Layer Z-Shaped Reflective Metasurface. *Electronics* **2023**, *12*, 2859. <https://doi.org/10.3390/electronics12132859>

Academic Editor: Yahya M. Meziari

Received: 28 April 2023

Revised: 11 June 2023

Accepted: 13 June 2023

Published: 28 June 2023



Copyright: © 2023 by the authors. Licensee MDPI, Basel, Switzerland. This article is an open access article distributed under the terms and conditions of the Creative Commons Attribution (CC BY) license (<https://creativecommons.org/licenses/by/4.0/>).

have presented several improved planar reflectors for the generation of OAM waves based on the generalized laws of reflection and refraction [13–16]. In addition, with the development of the universal theory on surface electromagnetics, a metasurface is applied to the current microwave and RF fields, which is a great step forward. A metasurface has many advantages as an important OAM waves generator, which are also applied to the design of OAM waves, such as the generation of OAM waves by adjusting the geometric parameters of the unit structure [17,18], and through the thermally tunable metasurface that reconstructs the operating frequency by changing the ambient temperature without changing the physical characteristics of the components [19–21]. The metamaterials of a metasurface are typical artificial structural materials based on subwavelength structures [22]. A metasurface is a uniform rectangular array (URA) with multiple low-cost passively reflective elements [23].

To address the low efficiency problem, multilayer structures and all-dielectric metasurfaces for various wavefront processing applications have been proposed and intensively studied. Grady et al. designed a three-layered metasurface, which could realize polarization conversion and the anomalous refraction of linearly polarized waves in the terahertz band [24]. Fan et al. proposed a tri-layered chiral structure metasurface, and broadband and high-efficiency cross-polarization conversion could be achieved in the range of 1.0 THz to 1.4 THz [25]. Shuang et al. explored a low-cost 2-bit programmable encoding metasurface and proposed an efficient optimization algorithm for generating high-order OAM waves [26].

Since terahertz technology has a great potential in high-speed wireless communications [27], terahertz OAM technology that combines terahertz and OAM is also a research hotspot. Terahertz technology typically involves the electromagnetic waves whose frequencies fall within the range of 0.1 to 10 THz [28]. Furthermore, terahertz OAM technology has been applied in various dynamic areas, including electron acceleration, high-definition terahertz imaging, and quantum state control [29–31].

In this paper, a broadband and efficient three-layer Z-shaped reflective metasurface for linear polarization conversion is designed, and six different modes of orbital angular momentum (OAM) waves are generated in the terahertz band. It could generate OAM waves with the modes ± 1 , ± 2 , and ± 3 . It is worth mentioning that the ± 3 mode is difficult to generate with traditional methods; however, it is easier to generate with a multilayer metasurface. The metasurface consisted of three-layer Z-shaped units. Each unit consisted of metal substrates separated by polyimide layers. By rotating the metal pattern, twelve different regions are obtained, and the metasurface could generate OAM waves with multiple modes by changing the structural parameters of the units. The reflection amplitude of the metasurface unit is more than 0.9 in the frequency range of 1.0 THz to 1.8 THz. The metasurface is illuminated by 1.0 THz to 1.8 THz circularly polarized waves to generate OAM waves with different modes (mode ± 1 , ± 2 , and ± 3). The far-field pattern, phase, and amplitude of the metasurface are obtained. Finally, the purity of the OAM waves of different modes is analyzed. The research in this paper improves the transmission efficiency and bandwidth of metasurfaces, and it has certain contributions and reference significance for the design of efficient broadband multi-functional metasurface OAM wave generators.

2. Metasurface Design

Recently, there have been many studies focused on nonlinear metasurfaces, dynamically tunable metasurfaces, and so on [19–21]. Although a dielectric metasurface is superior to a metallic metasurface due to its lower losses, more sophisticated fabrication techniques are required to create dielectric metasurfaces, especially when multiple dielectric materials and small size components are involved. Therefore, a metasurface is employed in this paper to generate broadband OAM waves in the terahertz band.

2.1. Unit Structure Design

Many studies have shown that the effect of using a single-layer structure in the terahertz band is not good. When a multi-layer structure is employed, it can generate OAM waves more efficiently. Thus the multi-layer structure is adopted in this paper. After several attempts and experiments, two better three-layer structure metasurfaces are designed. Figure 1 shows the schematic pattern of the proposed Z-type metasurface unit. The metasurface unit is composed of a metal substrate, a dielectric layer, and a Z-type patch layer structure. The bottom layer of the unit is a copper plate, behind which the control circuit is connected. It consists of metal sheets with a length of $p_l = 100 \mu\text{m}$, a width of $p_w = 100 \mu\text{m}$, and a thickness of $H_b = 0.2 \mu\text{m}$. The middle layer is composed of a polyacetamide dielectric layer with a cube structure, whose length is $100 \mu\text{m}$, width is $100 \mu\text{m}$, and height is $25 \mu\text{m}$. The top is the patch layer of the Z-shaped structure. The length of the middle part of the Z-shaped structure is $a = 60 \mu\text{m}$, the width is $w = 20 \mu\text{m}$, and the thickness is $tm = 0.2 \mu\text{m}$. The two ends of the Z-shaped structure are two identical structures with lengths of $b = 25 \mu\text{m}$, widths of $w = 20 \mu\text{m}$, and thickness measurements of $tm = 0.2 \mu\text{m}$. Figure 2 shows the schematic pattern of the proposed S-type metasurface unit. The metasurface unit is composed of a metal substrate, a dielectric layer and an S-type patch layer structure. It differs from the Z-type metasurface unit in the top layer, which is the patch layer of the S-type structure. The length of the middle part of the patch layer of the S-type structure is $a = 60 \mu\text{m}$, the width is $w = 20 \mu\text{m}$, and the thickness is $tm = 0.2 \mu\text{m}$. The two ends of the S-type structure are two three-quarter cylinder structures with the center at the vertex of the middle segment, the radius is $r = 20 \mu\text{m}$, and the thickness is $tm = 0.2 \mu\text{m}$. The angle is an important variable to be discussed in this paper and changing the rotation angle can produce a sudden phase change, which thus forms a phase difference. The metal materials used in this structure are all copper films with a conductivity of $\sigma = 5.8 \times 10^7 \text{ s/m}$, which can have a good effect. The dielectric layer is a polyacetamide dielectric layer with a square structure as shown in the gray parts in Figures 1 and 2.

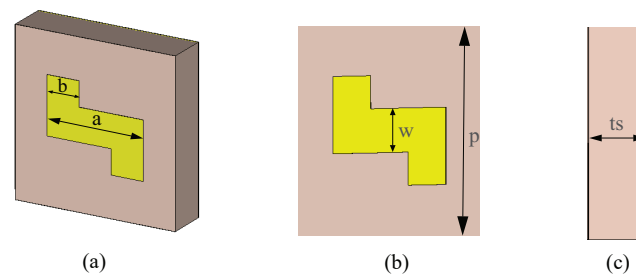


Figure 1. Z-type metasurface unit structure: (a) side view; (b) front view; (c) right view.

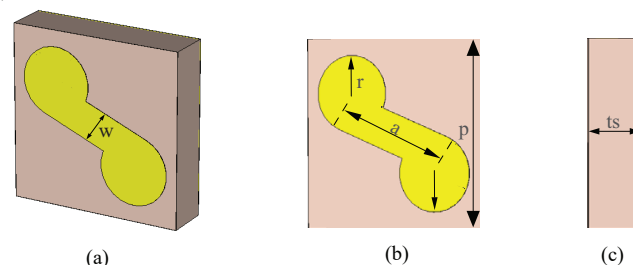


Figure 2. S-type metasurface unit structure: (a) side view; (b) front view; (c) right view.

For the simulation of this design, the polyimide with a dielectric constant of 3.5 and a loss tangent of 0.0027 is selected as the medium, which can produce better results. It should be noted that the patch layer structure is responsible for generating a polarization conversion and phase shift, while the two-layer structure of the latter layer is mainly responsible for the selection of linear polarization.

In this design, by adjusting the size of the structural parameters, the phase different that hardly changes with the frequency can be obtained in a wide frequency band, since the phase difference among the metasurface units remains basically unchanged in the range of 0.8 to 2.0 THz. Therefore, the gradient metasurface composed of this unit can realize ultra-broadband anomalous refraction, and then a discontinuous gradient distribution in the full phase range of 0 to 2π can be obtained. For the element model proposed in this paper, the simulation is carried out using the frequency domain solver in a electromagnetic field simulation software.

2.2. Design of Structural Parameters

In the simulation, the parameter angle is set as a variable, and a large amount of data is tested using the CST Microwave Studio, CST STUDIO SUITE 2019. Finally, a structure of twelve units with different parameters is found to have better performance in the range of 0.8 to 2.0 THz, where the first six metasurface units corresponded to angular parameter values of 0° , 30° , 60° , 90° , 120° , and 150° , and the last six structures are relative to the first six unit structures rotated 180° counterclockwise.

For the Z-type metasurface analysis, the frequency range is set to 0.8 to 2.0 THz, and Figure 3a shows the structure of these six metasurface units. The frequency of 0.8–2.0 THz is shown in Figure 3b, and the reflection amplitudes in the range of 1.0 THz to 1.8 THz are more than 0.9. According to the different parameters, the phase of each of the two metasurface units suddenly changed to 30° in the desired frequency range, and it is found that the phase difference hardly changed with the change in frequency. Figure 3c shows the phase and reflection amplitude at the center frequency of 1.4 THz. It can be seen that the phase difference of every two adjacent metasurface units is $\pi/6$, the six RIS unit structures could realize 2π phase coverage, and the reflection amplitudes in the range of 1.0 THz to 1.8 THz are all more than 0.9. The results show that the designed Z-type metasurface unit has good structural performance, which indicates the effective of the design.

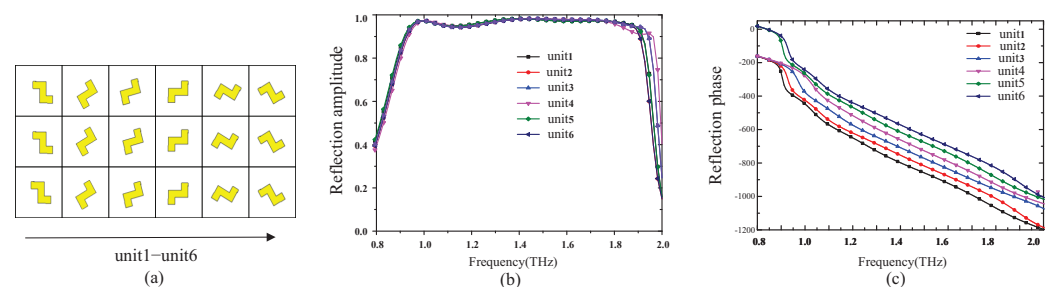


Figure 3. Performance analysis of Z-type elements with different structural parameters: (a) six metasurface unit structures; (b) reflection amplitude simulation results; (c) reflection phase at different frequencies.

Compared with the designed Z-type structure, the reflection amplitude of the S-type structure shown in Figure 4 is more than 0.9 in a short bandwidth, and it showed a small amplitude jump in the range of 1.0 THz to 1.8 THz. The reflection amplitude jump is more serious in the range of 1.6 to 2.0 THz, which affects the overall effect of the OAM waves generator. The results of reflected phase are shown in Figure 4c in the range of 1.0 to 1.6 THz. The phase difference between different units is 45° , however, the phase difference between different units is distorted after 1.6 THz. Compared to the effect of the Z-structured metasurface unit, the S-shaped structural unit is greatly reduced. In comparison of the effects of the Z-shaped and S-shaped units, the Z-shaped metasurface unit is shown to have a better effect, and it is finally selected to form the metasurface.

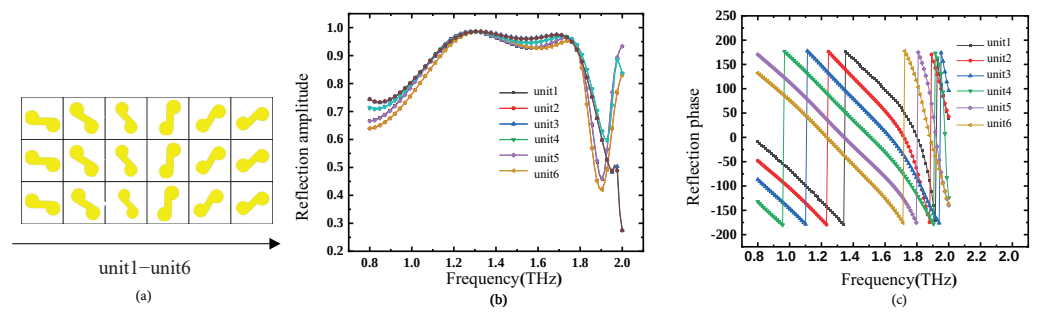


Figure 4. Performance analysis of S-type elements with different structural parameters: (a) six metasurface unit structures; (b) reflection amplitude simulation results; (c) reflection phase at different frequencies.

2.3. Design of Metasurface

Figure 5a,b illustrate the functional schematic of the metasurface under the left-handed circularly polarized (LHCP) wave and right-handed circularly polarized (RHCP) wave incidences, respectively. It consists of an array of units, as shown in Figure 5c.

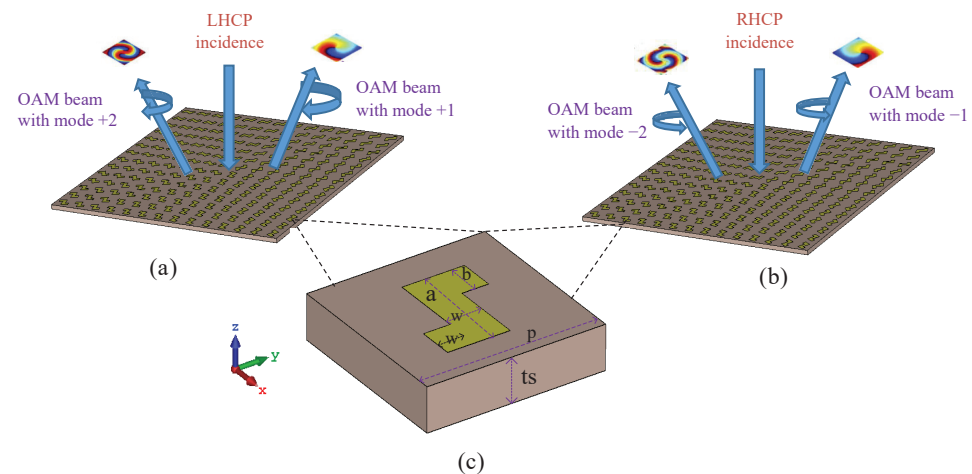


Figure 5. Functional schematic pattern of different circularly polarized terahertz beam incidences: (a) the schematic pattern before and after the incident of the LHCP wave; (b) the schematic pattern before and after the incident of the RHCP wave; (c) the schematic pattern of the structure of a single unit.

According to the geometric phase principle, twelve different metasurface units are designed by adjusting the different orientation angles of the top metal geometry to generate OAM waves on the metasurface. With the vertical central axis of the structure as the rotation axis, the phase shift of the OAM waves can be obtained by changing the structural parameters of the units under the incidence of a circularly polarized wave. The phase distribution carrying the OAM waves is $e^{jl\theta}$, where l is the mode number, and θ is the azimuth. In order to generate the desired OAM waves phase profile, the azimuth around the center point that the required phase distribution at each unit location needs to satisfy is given as the following equation:

$$\theta(x, y) = l \times \arctan\left(\frac{y}{x}\right), \tag{1}$$

where $\theta(x, y)$ represents the phase that satisfies the unit position, and l represents the desired OAM mode. Different modes are designed to generate OAM waves based on different phase arrangements of the metasurface. To simplify the proposed metasurface

design, the metasurface is divided into twelve triangular regions. The desired phase distribution of each region can be determined as follows:

$$\theta_l(x, y) = \frac{2\pi}{N} \left\{ l \times \frac{\tan^{-1}\left(\frac{y}{x}\right)}{\frac{2\pi}{N}} + 1 \right\}, \quad (2)$$

where N is the total number of regions divided around the center, and the modes number l is equal to an arbitrary integer. By adjusting the rotation angle of the metasurface through the design of the phase distribution value can generate OAM waves with different modes in the terahertz band. The metasurface is divided into structures as shown in Figure 6.

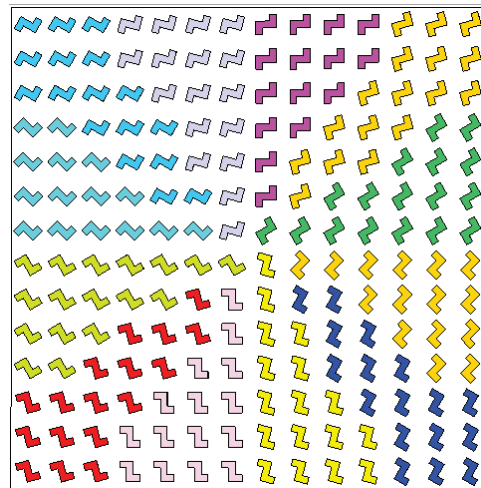


Figure 6. Element distributions of Z-shaped reflective metasurface.

3. Simulation and Analysis

According to the model constructed in Section 2, the simulation work is carried out in CST Microwave Studio, the relevant data obtained in CST Microwave Studio is imported into MATLAB, and its amplitude pattern, spectrum pattern, and mode purity pattern are obtained. According to the analysis in Section 2, the optimal parameters are derived, as are shown in Table 1.

Table 1. Simulation optimization parameters.

Simulation Parameters	Parameter Value
Sweep frequency range	0.8–2.0 THz
Gaussian plane beam frequency	1.0, 1.4, 1.8 THz
Distance between plane beam and metasurface	500 μm
Far-field observation distance	2000 μm
Dielectric constant	3.5
Dielectric layer loss tangent	0.0027
Conductivity of metal layer	$\sigma = 5.8 \times 10^7$ s/m

The procedure as follows: open the CST Microwave Studio according to the optimized parameters in Table 1. The unit structure is then constructed according to the relevant parameters of the metasurface unit, as shown in Figure 7a. According to the phase distribution of the metasurface in Section 2, divide the entire plane into twelve triangles to form the entire metasurface. Its arrangement structure is shown in Figure 7b according to the optimized parameters. Each triangular area is shown in Figure 7c, which constitutes a transmission-phase-type metasurface, and adjust the geometric phase of each unit area according to different modes to form the phase distribution required by the OAM waves. The analysis in Section 2 and the performance of the metasurface unit is proven, and the next step is to build a metasurface for simulation analysis.

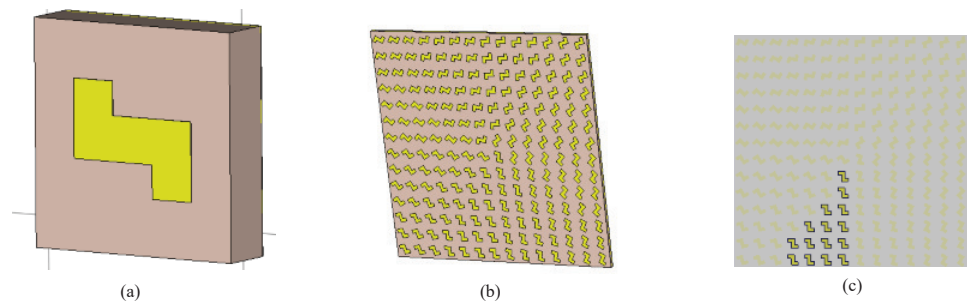


Figure 7. Phase distributions of metasurface: (a) metasurface unit; (b) the overall structure of the metasurface; (c) metasurface single area.

The frequency range is set from 0.8 to 2.0 THz, and a free space field is used whose length and width are the same as those of the metasurface; its height is $s = 2000 \mu\text{m}$, and the constructed field is shown in Figure 8a. The boundary conditions of the field, such as X and Y, are open, except that the minimum value of Z_{min} is electric ($E_t = 0$), and the observation field is a free field. The Z_{min} is set as an electrical boundary to facilitate the reflection of electromagnetic waves; the free space field is shown in Figure 8b. The next steps are to set up a Gaussian beam in CST Microwave Studio, and the incident signal parameters are set as follows: The frequencies of 1.0 THz, 1.4 THz and 1.8 THz selected for simulation respectively. The beam diameter and the distance between the beam and metasurface are both defined as $500 \mu\text{m}$; this is also the transmission direction towards metasurface. The left-polarized beam and right-polarized beam are selected according to the different modes, and the field intensity is set by default. When the signal source is added, the model in the CST Microwave Studio is shown in Figure 8c.

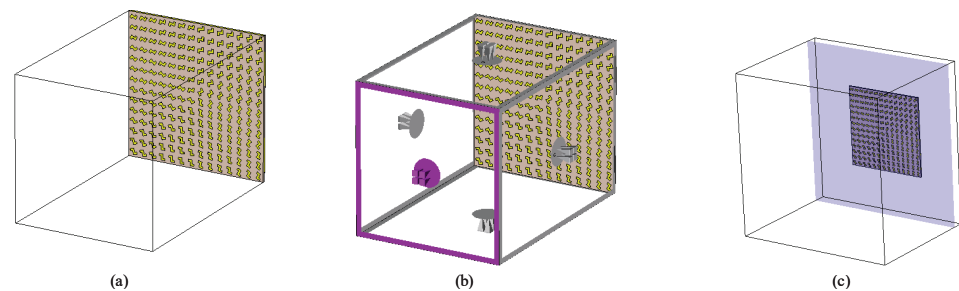


Figure 8. Free space field structure: (a) built free space field; (b) field boundary conditions; (c) the model after adding Gaussian signal.

The frequencies are selected as 1.0 THz, 1.4 THz, and 1.8 THz for simulation. The beam diameter and the distance between the beam and the metasurface are both $500 \mu\text{m}$. Transmission in the direction of the metasurface, the LHCP wave, and the RHCP wave are selected according to the different modes, and the field strength is set by default. The blue part is the Gaussian signal beam. Next, the simulation is carried out according to different frequencies and different modes. A far-field observer is added after the above steps for observing the far field. The results and analysis are as follows.

3.1. Wave Simulation Analysis of ± 1 Mode

In order to generate the OAM waves with the mode of $l = +1$, it is necessary to form a periodic phase distribution, which required phase distribution for the phase interval maintained at $\pi/6$ by the adjacent regions. Since the reflection amplitudes in the range of 1.0 THz to 1.8 THz in the above analysis are all above 0.9, three different frequencies of 1.0 THz, 1.4 THz and 1.8 THz are selected to analyze the effect of the OAM waves with the +1 mode. Twelve metasurface elements with different parameters are regularly placed in the entire plane, and the far-field and near-field results of the simulation are shown in Figure 9.

Figure 9 shows the far-field, near-field phase distribution, and amplitude pattern at different frequencies when the LHCP terahertz waves are irradiated on the surface of the designed metasurface. From the far-field radiation pattern in Figure 10, it can be seen that when the metasurface is adjacent $\pi/6$ to the phase-spaced region, OAM waves are generated at broadband frequencies of 1.0 THz to 1.8 THz. The second row shows the phase distribution, and the third row shows the amplitude. For $l = +1$, the data results are imported into MATLAB, and the ratio of the main mode power divided by the total power of all modes is used to obtain the main mode purity of the OAM waves at the three different frequencies when the mode $l = +1$. As shown in Figure 10, it can be seen that, under the irradiation of the left-handed polarization waves, the purity of the reflected OAM waves in its main mode purity exceeded 90%, thereby the result shown the designed metasurface has good performance for generating OAM waves with the mode of $l = +1$.

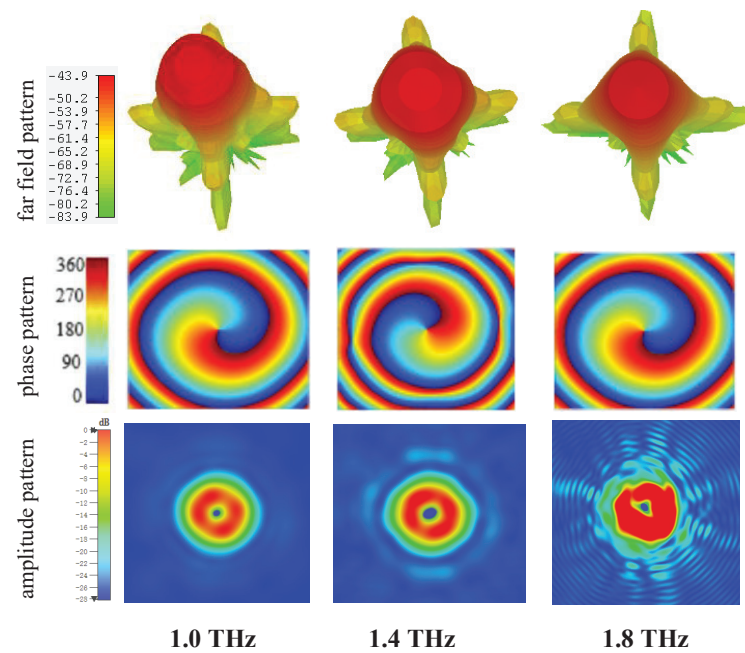


Figure 9. Far-field and near-field results of OAM waves with the mode +1 at different frequencies for the left-handed polarized wave incidence.

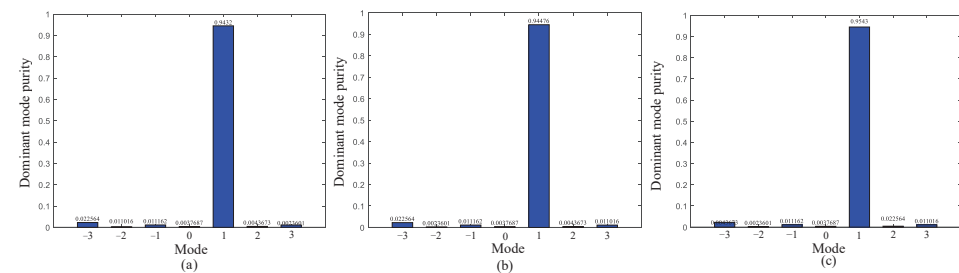


Figure 10. The purity of the dominant mode +1 at three different terahertz frequencies: (a) 1.0 THz; (b) 1.4 THz; (c) 1.8 THz.

The phase distribution required for the generation of OAM waves with the mode of $l = -1$ is exactly the opposite of the phase distribution of $l = +1$, in which the adjacent regions maintained a $\pi/6$ phase interval. There are two ways to realize OAM waves with the mode of -1 . The first method is to change the phase distribution of the twelve parts of the metasurface, which is opposite to the phase distribution in the case of $l = +1$, and it also uses a left-handed wave incident. Another method is to keep the phase distribution of the metasurface unchanged. With the right-handed polarized waves incident, the effects brought by the two methods are the same. Similarly, three different frequencies of 1.0 THz,

1.4 THz, and 1.8 THz are selected to analyze the effect of the OAM waves with the mode of -1 . From the far-field radiation pattern in Figure 11, it can be seen that, when the metasurface is adjacent to the phase interval region, OAM waves are generated at the broadband frequency of 1.0 THz to 1.8 THz. From the near-field phase distribution, it can be found that there is a spiral phase distribution characteristic when the mode $l = -1$. As shown in Figure 12, it can be seen that under the irradiation of the right-handed polarization waves, the mode purity of the reflected OAM waves exceeded 90%. The result shown that the designed metasurface has good performance for generating OAM waves with the mode of -1 .

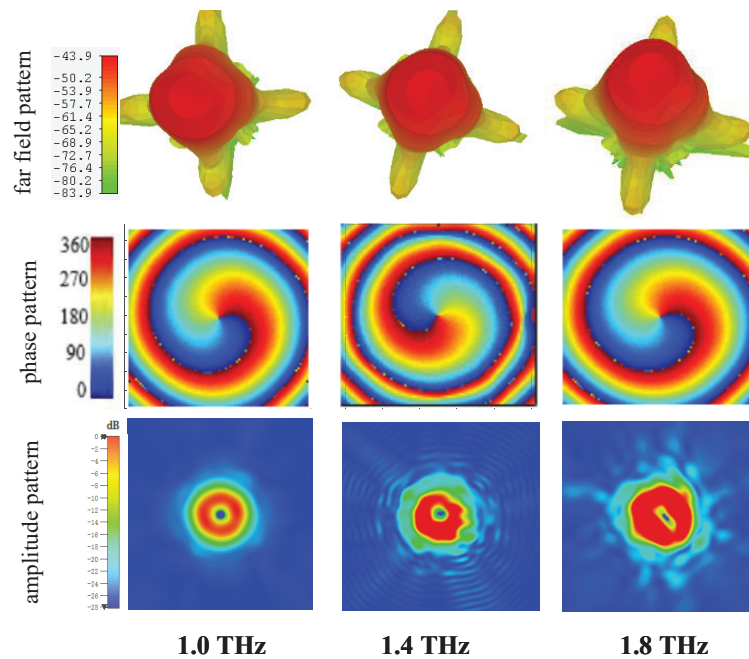


Figure 11. Far-field and near-field results of OAM waves with the mode -1 at different frequencies for right-handed polarized wave incidence.

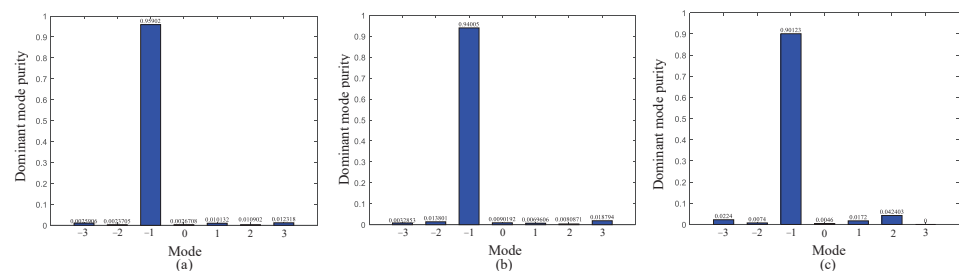


Figure 12. The purity of the dominant mode -1 at three different terahertz frequencies: (a) 1.0 THz; (b) 1.4 THz; (c) 1.8 THz.

3.2. Wave Simulation Analysis of ± 2 Mode

In order to generate the OAM waves with the mode of $l = \pm 2$, the phase interval should maintain $\pi/3$ in adjacent areas. The amplitude diagrams and phase distribution diagrams at frequencies of 1.0 THz, 1.4 THz, and 1.8 THz are shown in Figure 13. As can be seen from the far-field radiation diagrams in Figure 14, when the metasurface is adjacent to the $\pi/3$ phase interval, OAM waves are generated at broadband frequencies of 1.0 THz to 1.8 THz. From the near-field phase distribution, it can be found that there is a spiral phase distribution characteristic when the mode $l = +2$. The data results are imported into MATLAB, and the ratio of the main mode power divided by the total power of all modes is used to obtain the main mode purity of the OAM waves at the three different frequencies when $l = +2$, as shown in Figure 14. It can be seen that, under the irradiation of the

left-handed polarization waves, the purity of the reflected OAM waves in its mode purity exceeded 90%, thus the result shown that the designed metasurface has good performance for generating OAM waves with the +2 mode.

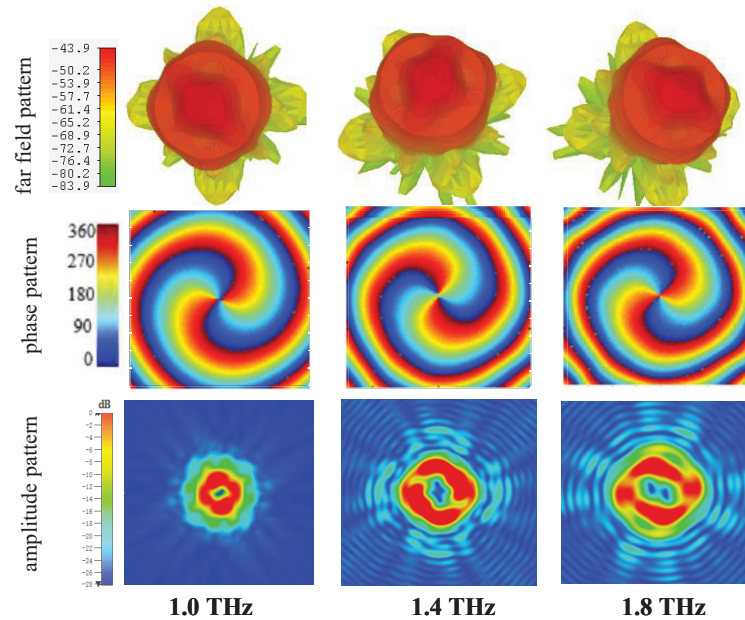


Figure 13. Far-field and near-field results of OAM waves with the +2 mode at different frequencies for left-handed polarized wave incidence.

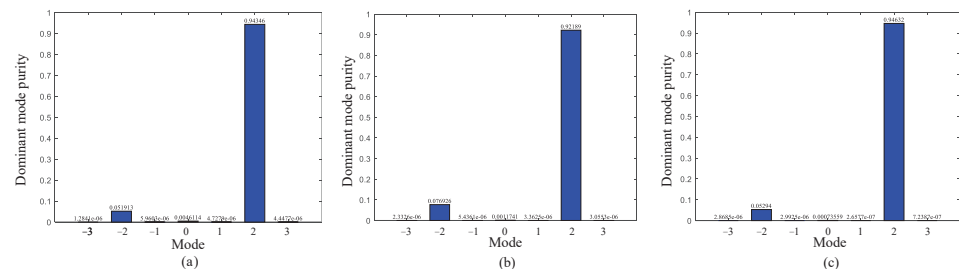


Figure 14. The purity of the dominant +2 mode at three different terahertz frequencies: (a) 1.0 THz; (b) 1.4 THz; (c) 1.8 THz.

The method of generating OAM waves with the mode $l = -2$ is the same as the mode of $l = +2$, which keeps the phase distribution of the metasurface unchanged or uses the right-handed polarized waves to enter the waves. The effects brought by the two methods are the same. Three different frequencies of 1.0 THz, 1.4 THz, and 1.8 are selected to analyze the OAM waves effect for the mode $l = -2$. The results of the far-field and near-field are shown in Figure 15. From the far-field radiation diagrams in Figure 15, it can be seen that, when the metasurface is adjacent to the $\pi/3$ phase interval, OAM waves are generated at broadband frequencies of 1.0 THz to 1.8 THz. From the near-field phase distribution, it can be found that there is a spiral phase distribution characteristic when the mode $l = -2$. There are distortions in the amplitude and phase distribution pattern at 1.8 THz, which may have been caused by interference at high frequencies, which needs to be improved in future work. When $l = -2$, as shown in Figure 16, it can be seen that, under the irradiation of the left-handed polarization waves, the purity of the reflected OAM waves in its mode purity exceeded 90%, thus the result shown that the designed metasurface has good performance for generating OAM waves with the mode of -2 .

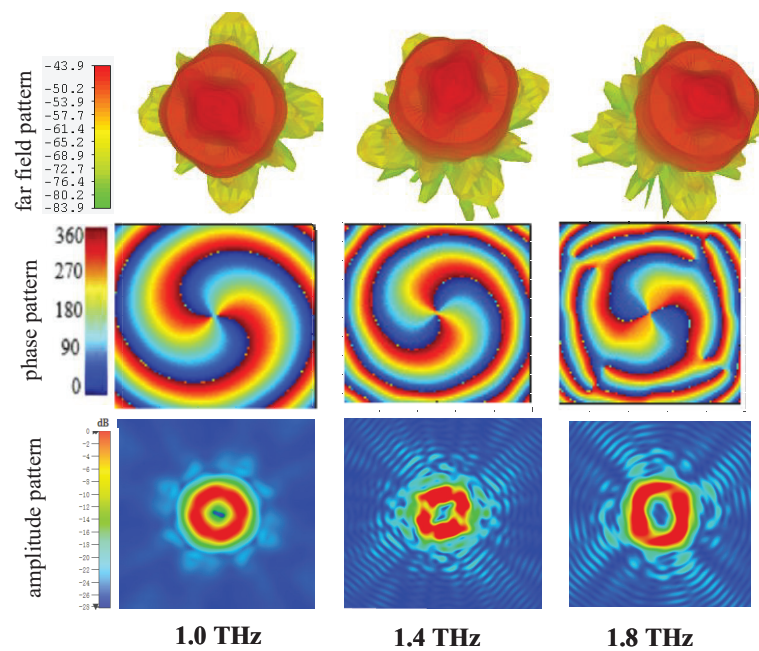


Figure 15. Far-field and near-field results of OAM waves with the -2 mode at different frequencies for right-handed polarized wave incidence.

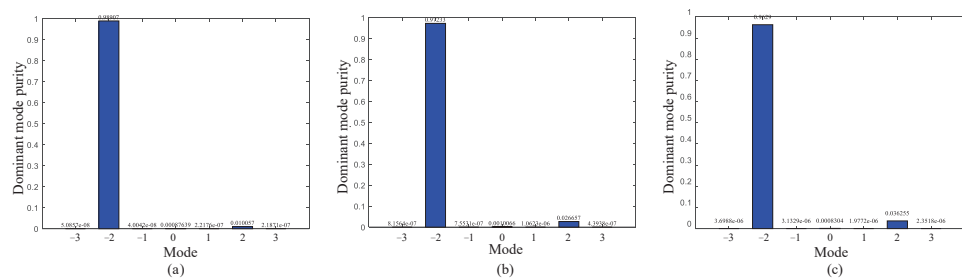


Figure 16. The purity of the dominant -2 mode at three different terahertz frequencies: (a) 1.0 THz; (b) 1.4 THz; (c) 1.8 THz.

3.3. Wave Simulation Analysis of ± 3 Mode

When realizing the four modes of ± 1 and ± 2 , the designed metasurface is employed to generate OAM waves for ± 3 modes. The OAM waves mode of ± 3 produced the required phase distribution to maintain a $\pi/2$ phase interval. The terahertz frequencies of 1.0 THz, 1.4 THz, and 1.8 THz are selected for the analysis of the metasurface. The results of the far-field and near-field are shown in Figure 17. From the far-field diagrams in Figure 17, it can be seen that, when the metasurface is adjacent to the $\pi/2$ phase interval, OAM waves are generated at the three different terahertz frequencies. From the near-field phase distribution, it can be found that there is a spiral phase distribution characteristic when the mode $l = +3$.

The data results are imported into MATLAB, and the ratio of the main mode power divided by the total power of all modes is used to obtain the main mode purity of the OAM waves at the three different frequencies when $l = +3$, as shown in Figure 18. It can be seen that, under the irradiation of the left-handed polarization waves, the reflected OAM waves have a high purity in its mode, which is more than 80% at 1.0 THz and 1.4 THz, however its purity is reduced compared with the $l = \pm 1$ and $l = \pm 2$ modes. In the simulation, it is found that this part of the problem is mainly caused by the mutual echo interference between several areas of the metasurface. When the number of modes increased, the interference is more serious. Compared with the traditional OAM waves generator, the proposed metasurface could achieve a mode purity of 80%.

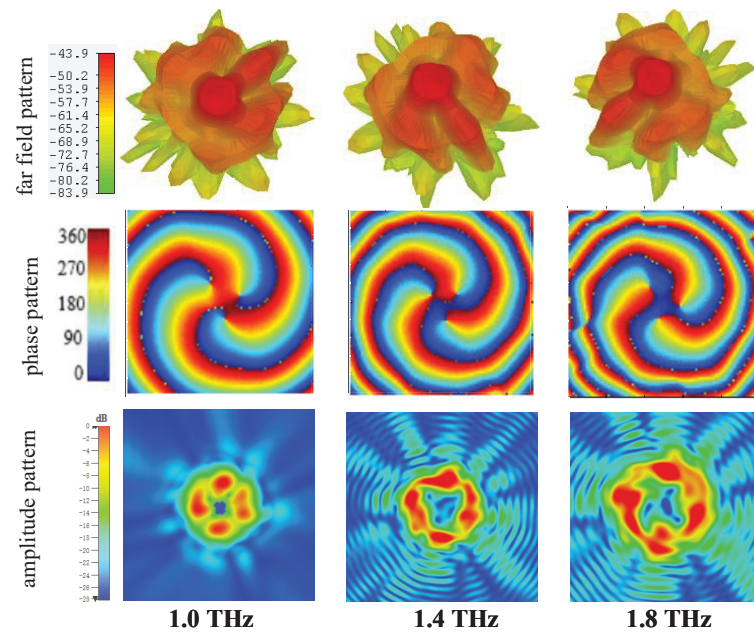


Figure 17. Far-field and near-field results of OAM waves with the +3 mode at different frequencies for left-handed polarized wave incidence.

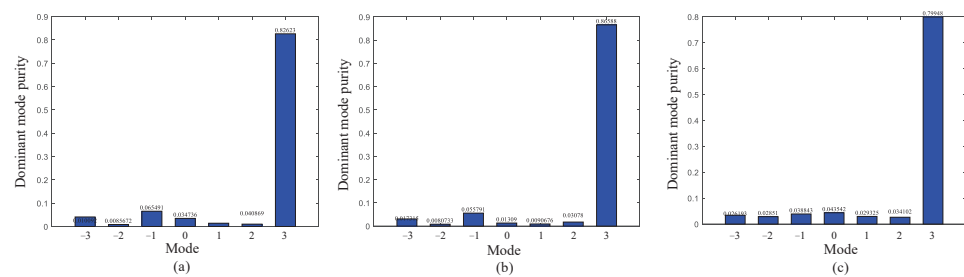


Figure 18. The purity of the dominant +3 mode at three different terahertz frequencies: (a) 1.0 THz; (b) 1.4 THz; (c) 1.8 THz.

The implementation of $l = -3$ is consistent with the two methods of the -1 and -2 modes, which keep the phase distribution of the metasurface unchanged and used a right-handed polarized waves incident; the effects of the two methods are consistent. Similarly, three different frequencies of 1.0 THz, 1.4 THz and 1.8 THz are selected to analyze the effects of -3 mode OAM wave. Twelve metasurface element models with different parameters are regularly placed in the whole model. The results of the far-field and near-field are shown in Figure 19. When the metasurface is adjacent to the $\pi/2$ phase interval, OAM waves are generated at the three different terahertz frequencies. From the near-field phase distribution, it can be found that there is a spiral phase distribution characteristic when the mode $l = -3$. As shown in Figure 20, it can be seen that under the irradiation of the left-handed polarization waves, the reflected OAM waves have a high purity mode when $l = -3$. The result shown that the designed metasurface have better performance in generating OAM waves with the -3 mode compared to the traditional method.

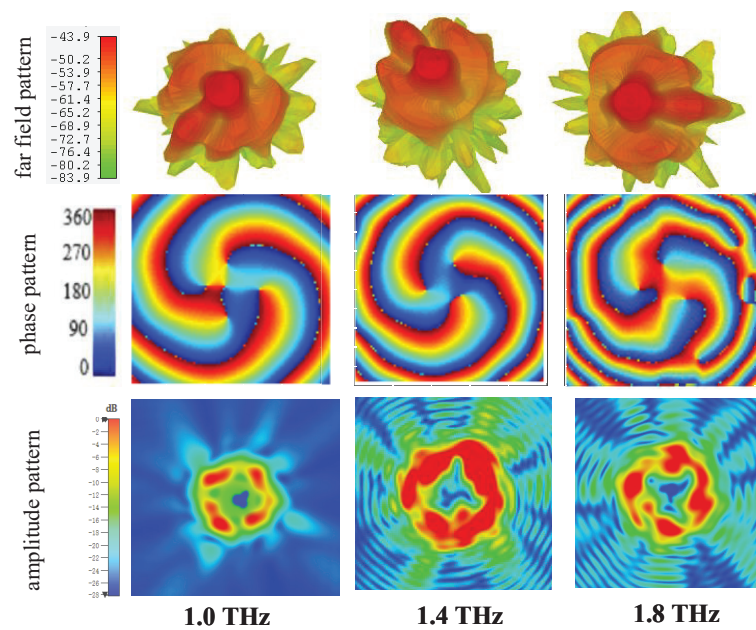


Figure 19. Far-field and near-field results of OAM waves with the -3 mode at different frequencies for right-handed polarized wave incidence.

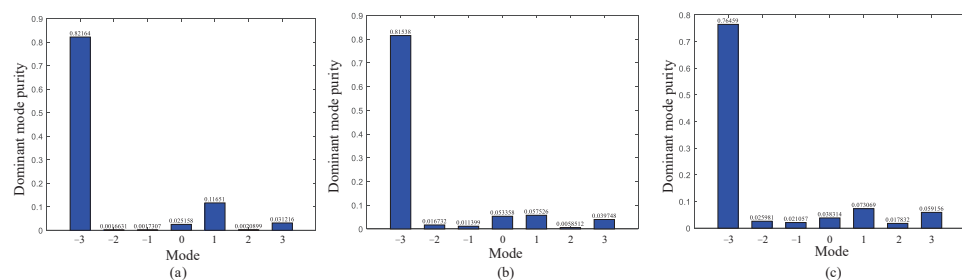


Figure 20. The purity of the dominant -3 mode at three different terahertz frequencies: (a) 1.0 THz; (b) 1.4 THz; (c) 1.8 THz.

4. Conclusions

In this paper, a design method of a terahertz broadband OAM waves generation based on a metasurface is proposed. The designed metasurface consist of a metal patch layer and a metal substrate separat by a polyimide substrate. During the design process, the metasurface unit is first designed. The design of three-layer metal patch layer structure of metasurface is studied and S-type unit and Z-type unit are compared and analyzed. Compared with the S-type unit, the Z-type unit has better performance. The reflection amplitude of the Z-type unit is more than 0.9 in the range of 1.0 THz to 1.8 THz. By changing the rotation angle of the patch unit, the phase difference of every two metasurface units in the ideal frequency domain is a fixed value, and it do not change with the frequency change; thus, then the range 0 to 2π of the OAM waves phase could be achieved. The metasurface units are arranged in a specific order to form a metasurface, which converted the incident planar linearly polarized waves into OAM waves. OAM terahertz waves with six modes of ± 1 , ± 2 , and ± 3 are generated under the irradiation of Gaussian beams at 1.0 THz, 1.4 THz, and 1.8 THz, respectively, and the main purity of the generated OAM waves is higher than 70%; the four modes ± 1 and ± 2 are exceed 90% at the main mode purity, thereby the reliability and broadband characteristics of the OAM-waves-generator-based metasurface is confirmed.

Author Contributions: Funding acquisition, Q.Z.; Methodology, N.Z., L.Y.; Software, X.X.; Supervision, Q.Z.; Visualization, X.X.; Writing—original draft, X.X.; Writing—review and editing, Q.Z. All authors have read and agreed to the published version of the manuscript.

Funding: This work is supported by the National Natural Science Foundation of China (Grant No. 61961024, 62261037) and the Natural Science Foundation of Jiangxi Province (Grant No. 20181BAB202001).

Data Availability Statement: No new data were created or analyzed in this study. Data sharing is not applicable to this article.

Acknowledgments: Thank Bin Luo for his support, help and discussion of this research.

Conflicts of Interest: The authors declare no conflict of interest.

Abbreviations

The following abbreviations are used in this manuscript:

OAM	Orbital Angular Momentum
OFDM	Orthogonal Frequency Division Multiplexing
LHCP	Left Hand Circular Polarization
RHCP	Right Hand Circular Polarization

References

1. Tang, P.; Zheng, X.; Ma, T.; Cheng, G.; Wu, G.; Bao, X.; Sun, H.; Ding, J.; Si, L. Terahertz Dual-Band Dual-Polarization 3-Bit Coding Metasurface for Multiple Vortex Beams Generation. *Electronics* **2023**, *12*, 1868 [CrossRef]
2. Ali, A.; Khalily, M.; Serghiou, D.; Tafazolli, R. Reflective Metasurface With Steered OAM Beams for THz Communications. *IEEE Access* **2023**, *11*, 12394–12401. [CrossRef]
3. Li, Q.; Wu, C.; Zhang, Z.; Zhao, S.; Zhong, B.; Li, S.; Li, H.; Jin, L. High-purity Multi-mode Vortex Beam Generation With Full Complex-Amplitude-Controllable Metasurface. *IEEE Trans. Antennas Propag.* **2023**, *71*, 774–782. [CrossRef]
4. Allen, L.; Beijersbergen, M.W.; Spreeuw, R.J.C.; Woerdman, J.P. Orbital Angular Momentum of Light and the Transformation of Laguerre-Gaussian Laser Modes. *Phys. Rev. A* **1992**, *45*, 8185–8189. [CrossRef]
5. Liu, K.; Liu, H.; Qin, Y.; Cheng, Y.; Wang, S.; Li, X.; Wang, H. Generation of OAM Beams Using Phased Array in the Microwave Band. *IEEE Trans. Antennas Propag.* **2016**, *64*, 3850–3857. [CrossRef]
6. Lee, I.; Sawant, A.; Choi, E. High-directivity Orbital Angular Momentum Antenna for Millimeter-Wave Wireless Communications. *IEEE Trans. Antennas Propag.* **2021**, *69*, 4189–4194. [CrossRef]
7. Yang, H.; Zheng, S.; He, W.; Yu, X.; Zhang, X. Terahertz Orbital Angular Momentum: Generation, Detection and Communication. *China Commun.* **2021**, *18*, 131–152. [CrossRef]
8. Tamburini, F.; Mari, E.; Sponselli, A.; Thidé, B.; Bianchini, A.; Romanato, F. Encoding Many Channels on The Same Frequency Through Radio Vorticity: First Experimental Test. *New J. Phys.* **2012**, *14*, 033001. [CrossRef]
9. Hui, X.; Zheng, S.; Hu, Y.; Xu, C.; Jin, X.; Chi, H.; Zhang, X. Ultralow Reflectivity Spiral Phase Plate for Generation of Millimeter-Wave OAM Beam. *IEEE Antennas Wirel. Propag. Lett.* **2015**, *14*, 966–969. [CrossRef]
10. Fouda, R.M.; Ebrahimi, A.; Baum, T.C.; Ghorbani, K. Experimental BER Performance of Quasi-Circular Array Antenna for OAM Communications. *IEEE Antennas Wirel. Propag. Lett.* **2020**, *19*, 1350–1354. [CrossRef]
11. Pan, Y.; Zheng, S.; Zheng, J.; Li, Y.; Jin, X.; Chi, H.; Zhang, X. Generation of Orbital Angular Momentum Radio Waves Based on Dielectric Resonator Antenna. *IEEE Antennas Wirel. Propag. Lett.* **2017**, *16*, 385–388. [CrossRef]
12. Wang, L.; Chen, H.; Guo, K.; Shen, F.; Guo, Z. An Inner- and Outer-Fed Dual-Arm Archimedean Spiral Antenna for Generating Multiple Orbital Angular Momentum Modes. *Electronics* **2019**, *8*, 251. [CrossRef]
13. Zelenchuk, D.; Fusco, V. Split-ring FSS Spiral Phase Plate. *IEEE Antennas Wirel. Propag. Lett.* **2013**, *12*, 284–287. [CrossRef]
14. Chen, M.L.N.; Jiang, L.J.; Sha, W.E.I. Quasi-Continuous Metasurfaces for Orbital Angular Momentum Generation. *IEEE Antennas Wirel. Propag. Lett.* **2019**, *18*, 477–481. [CrossRef]
15. Xu, H.-X.; Liu, H.; Ling, X.; Sun, Y.; Yuan, F. Broadband Vortex Beam Generation Using Multimode Pancharatnam–Berry Metasurface. *IEEE Trans. Antennas Propag.* **2017**, *65*, 7378–7382. [CrossRef]
16. Yu, S.; Li, L.; Shi, G. Dual-Polarization and Dual-Mode Orbital Angular Momentum Radio Vortex Beam Generated by Using Reflective Metasurface. *Appl. Phys. Express* **2016**, *9*, 082202. [CrossRef]
17. Yang, L.; Sun, S.; Sha, W. Ultrawideband Reflection-Type Metasurface for Generating Integer and Fractional Orbital Angular Momentum. *IEEE Trans. Antennas Propag.* **2020**, *68*, 2166–2175. [CrossRef]
18. Guo, K.; Zheng, Q.; Yin, Z.; Guo, Z. Generation of Mode-Reconfigurable and Frequency-Adjustable OAM Beams Using Dynamic Reflective Metasurface. *IEEE Access* **2020**, *8*, 75523–75529. [CrossRef]

19. He, B.; Fan, J.; Cheng, Y.; Chen, F.; Luo, H.; Gong, R. Thermally Tunable Terahertz Vortex Beam Generator Based on An InSb Metasurface. *J. Opt. Soc. Am. B* **2021**, *38*, 1518–1524. [[CrossRef](#)]
20. Yang, Q.; Wang, Y.; Liang, L.; Yang, M. Broadband Transparent Terahertz Vortex Beam Generator Based on Thermally Tunable Geometric Metasurface. *Opt. Mater.* **2021**, *121*, 111574. [[CrossRef](#)]
21. He, B.; Liu, J.; Cheng, Y.; Chen, F.; Luo, H.; Li, X. Broadband and Thermally Switchable Reflective Metasurface Based on Z-shape InSb for Terahertz Vortex Beam Generation. *Phys. E Low-Dimens. Syst. Nanostruct.* **2022**, *144*, 115373. [[CrossRef](#)]
22. Zheng, J.; Zhang, X.; Liu, L.; Li, Q.; Singh, L.; Han, J.; Yan, F.; Zhang, W. Tailoring Terahertz Propagation by Phase and Amplitude Control in Metasurfaces. *J. Infrared Millim. Terahertz Waves* **2017**, *38*, 1034–1046. [[CrossRef](#)]
23. Li, Y.; Jiang, M.; Zhang, G.; Cui, M. Achievable Rate Maximization for Intelligent Reflecting Surface-Assisted Orbital Angular Momentum-Based Communication Systems. *IEEE Trans. Veh. Technol.* **2021**, *70*, 7277–7282. [[CrossRef](#)]
24. Grady, N.K.; Heyes, J.E.; Chowdhury, D.R.; Zeng, Y.; Reiten, M.T.; Azad, A.K.; Taylor, A.J.; Dalvit, D.A.; Chen, H.T. Terahertz Meta-Materials for Linear Polarization Conversion and Anomalous Refraction. *Science* **2013**, *340*, 1304–1307. [[CrossRef](#)]
25. Fan, J.; Cheng, Y. Broadband High-Efficiency Cross-Polarization Conversion and Multi-Functional Wavefront Manipulation Based on Chiral Structure Metasurface for Terahertz Wave. *J. Phys. D Appl. Phys.* **2019**, *53*, 025109. [[CrossRef](#)]
26. Shuang, Y.; Zhao, H.; Ji, W.; Cui, T.J.; Li, L. Programmable High-Order OAM-Carrying Beams for Direct-Modulation Wireless Communications. *IEEE J. Emerg. Sel. Top. Circuits Syst.* **2020**, *10*, 29–37. [[CrossRef](#)]
27. Shuang, Y.; Zhao, H.; Ji, W.; Cui, T.J.; Li, L. 100 Gbit/s THz Photonic Wireless Transmission in The 350-GHz Band With Extended Reach. *IEEE Photonics Technol. Lett.* **2018**, *30*, 1064–1067.
28. Han, C.; Wang, Y.; Li, Y.; Chen, Y.; Abbasi, N.A.; Kürner, T.; Molisch, A.F. Terahertz Wireless Channels: A Holistic Survey on Measurement, Modeling, and Analysis. *IEEE Commun. Surv. Tutor.* **2022**, *24*, 1670–1707. [[CrossRef](#)]
29. Sanvitto, D.; Marchetti, F.M.; Szymańska, M.H.; Tosi, G.; Baudisch, M.; Laussy, F.P.; Krizhanovskii, D.N.; Skolnick, M.S.; Marrucci, L.; Lemaître, A.; et al. Persistent Currents and Quantized Vortices in A Polariton Superfluid. *Nat. Phys.* **2010**, *6*, 527–533. [[CrossRef](#)]
30. Kampfrath, T.; Tanaka, K.; Nelson, K.A. Resonant and Nonresonant Control Over Matter and Light by Intense Terahertz Transients. *Nat. Photon* **2013**, *7*, 680–690. [[CrossRef](#)]
31. Nanni, E.A.; Huang, W.R.; Hong, K.-H.; Ravi, K.; Fallahi, A.; Moriena, G.; Miller, R.J.D.; Kärtner, F.X. Terahertz-Driven Linear Electron Acceleration. *Nat. Commun.* **2015**, *6*, 8486. [[CrossRef](#)] [[PubMed](#)]

Disclaimer/Publisher’s Note: The statements, opinions and data contained in all publications are solely those of the individual author(s) and contributor(s) and not of MDPI and/or the editor(s). MDPI and/or the editor(s) disclaim responsibility for any injury to people or property resulting from any ideas, methods, instructions or products referred to in the content.